Energy transfer in Cr and Nd co-doped Si-B-Na-Al-Ca-Zr-O glasses

Hughes, MA, Li, H, Curry, RJ, Suzuki, T and Ohishi, Y

http://dx.doi.org/10.1016/j.jnoncrysol.2019.119769

Energy transfer in Cr and Nd co-doped Si-B-Na-Al-Ca-Zr-O glasses

M. A. Hughes[a]*, H. Li[a], R. J. Curry[b], T. Suzuki[c] and Y. Ohishi[c]

[a]*Joule Physics Laboratory, School of Computing, Science and Engineering, University of Salford, Salford, M5 4WT, UK;* [b]*Photon Science Institute, Department of Electrical and Electronic Engineering, University of Manchester, Manchester UK M13 9PL;* [c]*Research Center for Advanced Photon Technology, Toyota Technological Institute, 2-12-1 Hisakata, Tempaku, Nagoya 468-8511, Japan*

*Corresponding author: m.a.hughes@salford.ac.uk

Cr and Nd co-doped glasses are potential gain media for solar pumped lasers (SPLs). Tanabe-Sugano analysis shows that Cr doped Si-B-Na-Al-Ca-Zr-O (SBNACZ) glass contains a mixture of Cr^{3+} with octahedral coordination and Cr^{6+} with unknown coordination. The crystal field parameters for Cr^{3+} were Dq = 1574 cm^{-1}, B = 792.2 cm^{-1}, C = 3005 cm^{-1} and Dq/B = 1.99, indicating a low covalency of Cr-O bonds. We compared the quantum efficiency (QE) of Nd and Cr co-doped SBNACZ glass with Nd doped SBNACZ glass to determine the $Cr^{3+}\rightarrow Nd^{3+}$ transfer QE. The Cr_2O_3 content was fixed at 0.1 mol.% and the Nd_2O_3 content was varied between 0.1 and 1 mol.%. A maximum transfer QE of 20% was obtained at 0.5 mol.% Nd_2O_3. $Cr^{3+}\rightarrow Nd^{3+}$ energy transfer is dominated by the coulombic interaction mechanism. The clustering of Nd^{3+} was a limiting factor for increasing the transfer QE with higher Nd^{3+} concentrations.

Keywords: glass; chromium; neodymium; doping; optical spectroscopy; energy transfer

1. Introduction

The ability to store solar energy in order to match electricity demand is an increasing concern. To this end, solar pumped lasers (SPLs) have attracted attention. It has been proposed that SPLs may be used to store solar energy in the form of Mg by reducing MgO with a high intensity laser beam [1], and a 42.5% energy recovery efficiency for the reduction of MgO has been demonstrated [1].

The Nd^{3+} ion is one of the most commonly used active ions in solid-state laser materials. However, conversion efficiencies when lamp pumped tend to be low, for example lamp pumped Nd-doped yttrium aluminum garnet (Nd:YAG) has a conversion efficiency of only 2-3% [2]. This is because Nd^{3+} has relatively narrow absorption bands, so a large proportion of broadband excitation is not absorbed and is therefore wasted. A solution to this problem is to co-dope with Cr^{3+}. The Cr^{3+} ion has a broad absorption in the visible region, covering the emission spectra of halogen lamps, which may be used to sensitize Nd^{3+} via energy transfer from the $^4T_2 \rightarrow {}^4A_2$ transition of Cr^{3+} [2]. Using this sensitization strategy increases the output power of Cr and Nd^{3+} co-doped YAG by a factor of eight [3]. This approach for increasing broadband pump source absorption efficiency is also applicable to SPLs, and a few Cr and Nd^{3+} co-doped YAG SPLs have been demonstrated [2, 4].

In contrast to the use of crystalline and polycrystalline hosts for SPLs, the use of a glass host would provide significant advantages, including the ability to utilise fiber geometries for higher alignment stability and robustness, superior heat dissipation due to the large surface area to volume ratio of the optical fiber, and improved efficiency. SiO_2:B_2O_3:Na_2O:Al_2O_3:CaO:ZrO_2 (SBNACZ) glass was initially suggested as a host medium to immobilise high level nuclear waste [5]. It has excellent rare earth solubility, chemical durability and thermal stability, with no crystallisation observed when doped with rare earths up to 30 wt% [6]. This high rare earth solubility makes SBNACZ glass a promising candidate

host material to use when energy transfer from co-dopants is required and is therefore a potential candidate as a host medium for SPLs. There are only a few optical spectroscopy studies of doped SBNACZ glasses [6-8], and the spectroscopic properties and energy transfer for Cr and Nd doped SBNACZ glasses haven't been investigated.

In this study we report the absorption and emission spectra, quantum efficiency and fluorescence lifetime of Cr_2O_3 and Nd_2O_3 singly and co-doped SBNACZ glasses. We use these spectroscopic measurements to determine the valence and coordination of the Cr dopant, the $Cr^{3+} \rightarrow Nd^{3+}$ energy transfer efficiency, and transfer mechanism.

2. Experimental

SBNACZ glasses, 65.3-(x+y) SiO_2:14.2 B_2O_3:9.3 Na_2CO_3:4.4 Al_2O_3:3.5 $CaCO_3$:3.3 ZrO_2:x Cr_2O_3:y Nd_2O_3, (% molar) (x = 0 and 0.1; y = 0, 0.1, 0.5 and 1) were prepared for this study. The raw materials were mixed thoroughly using an alumina mortar and pestle, and then melted at 1500°C for 2 hours under an N_2 atmosphere in a platinum crucible. The glass melt was subsequently quenched by casting into a stainless steel mold preheated to 500°C. The quenched glass was finally annealed at 570°C for 4 hours, based on previous thermal measurements of SBNACZ glass [7].

A Perkin Elmer Lambda 900 spectrophotometer was used to take absorption spectra over a wavelength range of 175-3300 nm with a resolution of ±0.1 nm. The emission spectra were obtained by exciting at 455, 655 or 808 nm using laser diodes. The fluorescence was dispersed in a Jasco CT-25C monochromator with a slit width of ~2 mm and a 600 lines/mm grating blazed at 1000 nm, giving a spectral resolution of ~6 nm. The excitation laser was prevented from entering the monochromator using either a 680 or 850 nm long-pass filter. Detection was realised with a Hamamatsu visible photomultiplier tube (PMT) or a Hamamatsu

G5852-11 InGaAs detector, coupled with standard phase-sensitive detection. A correction spectrum, $C(\lambda)$, was used on all the emission spectra to take into account the wavelength dependent response of the measurement tool. $C(\lambda)=I_{WL}(\lambda)/I_{res}(\lambda)$, where $I_{WL}(\lambda)$ is the spectral luminance of an Ushio calibrated white light source, supplied by the manufacturer, $I_{res}(\lambda)$ is the measured response of the detection system to the input of the calibrated white light source. To ensure reproducibility and check sample homogeneity, measurements were obtained from at least three different positions of the sample. Cryogenic measurements were made by placing the sample in a closed-cycle He gas cryostat. Transient fluorescence measurements utilized the same tool used in emission measurements, except the transient signal was recorded on a Yokogawa DL1620 200MHz oscilloscope, averaged over ~10000 decays. The fluorescence decay profiles were non-exponential; therefore, lifetimes were calculated using the average lifetime function as expressed in Eq. (1) [9]

$$\tau = \frac{\int tI(t)}{\int I(t)} \tag{1}$$

where $I(t)$ is the fluorescence intensity and τ is the characteristic fluorescence lifetime.

The QE measurements were performed using the same system used for the emission measurements, but with the sample (~3×3×1 mm) placed in a Labsphere 4P-GPS-040-SF integrating sphere (diameter: ~10 cm). The sample was placed behind a baffle so that there was no direct optical path between the sample and the exit port. The sample was aligned so that the reflected excitation beam was directed well away from the entrance port, as described previously [10, 11]. We used a 'photons out/photons in' method, similar to that described previously [12, 13], to calculate the QE. The number of absorbed photons is specified as being proportional to the difference between the area of the spectrum of laser line with the sample present ($I_{sample}(\lambda)$) and without the sample present ($I_{sphere}(\lambda)$). The number of emitted photons is specified as being proportional to the area of the emission spectra ($I_{PL}(\lambda)$), see Fig. 7(a). These spectra were corrected for the system response with a correction spectrum ($C(\lambda)$). A

photon energy correction was also made, since a higher photon flux is required at longer wavelengths to produce the same spectral irradiance than at shorter wavelengths, by multiplying by the wavelength. Therefore, the QE can be expressed as:

$$\mathrm{QE} = \frac{\int \lambda I_{PL}(\lambda) C(\lambda) d\lambda}{\int \lambda I_{sphere}(\lambda) C(\lambda) d\lambda - \int \lambda I_{sample}(\lambda) C(\lambda) d\lambda} \quad (2)$$

3. Results and discussion

3.1. Cr-doped SBNACZ glass

Fig. 1 shows the absorption spectrum of 0.1 mol.% Cr_2O_3 doped SBNACZ glass displaying three broad absorption bands, characteristic of spin allowed transitions, centered at 360, 432 and 635 nm.

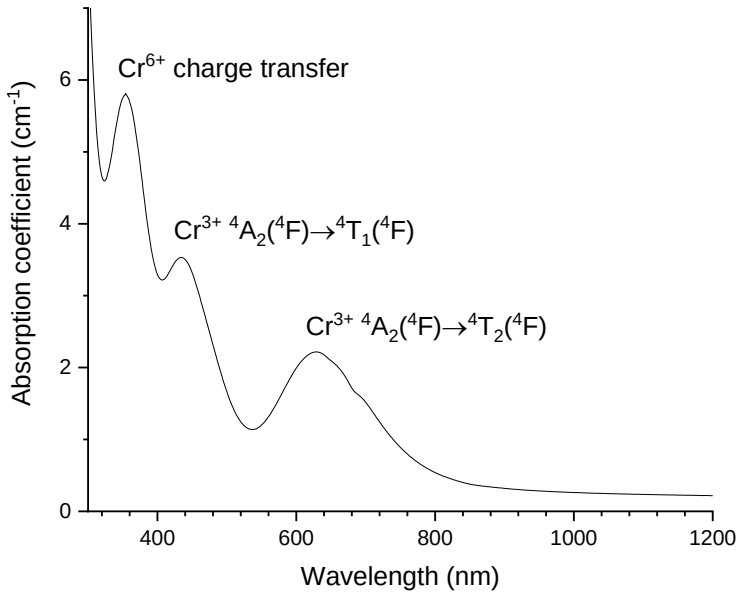

Figure 1. Absorption spectrum of 0.1 mol.% Cr_2O_3 doped SBNACZ glass.

The 635 nm absorption band is enlarged in Fig. 2. The two dips in this band result from the Fano antiresonance effect [14], which occurs when broad spin-allowed bands are superimposed in the same energy region as narrow spin-forbidden bands. To find the positions of the two

spin-forbidden bands, a Gaussian fit was performed for the 635 nm absorption band. The inset of Fig. 2 shows the Gaussian fit subtracted from the absorption band, thereby revealing the positions of the spin-forbidden bands to be at 649 and 681 nm, respectively.

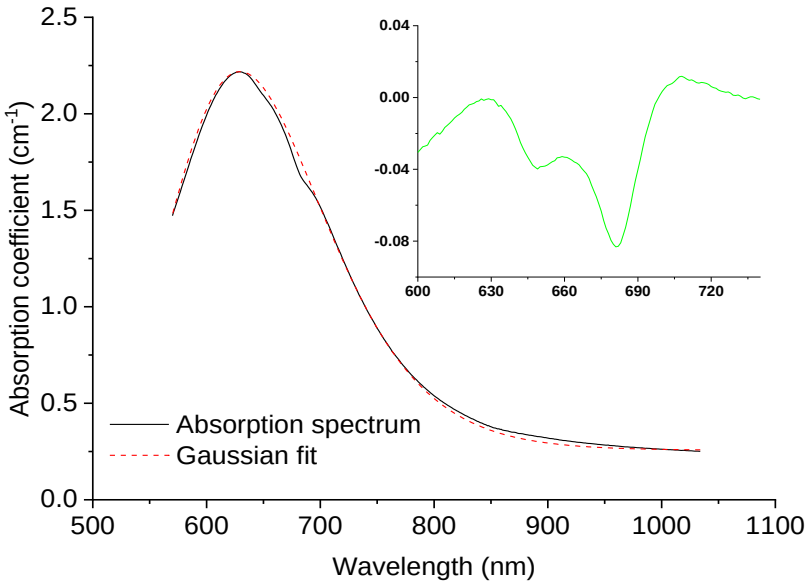

Figure 2. The 642 nm absorption band of Cr-doped SBNACZ glass, fitted with a Gaussian in terms of energy. The inset shows the Gaussian fit subtracted from the absorption spectrum.

In order to determine the oxidation state and coordination of the Cr ion, we performed Tanabe-Sugano analysis on the various possible oxidation state and coordination configurations of the Cr ion, in a similar manner to what we have performed previously on V doped chalcogenide glass [15]. Possible oxidation states for Cr are Cr^{6+}, Cr^{5+}, Cr^{4+}, Cr^{3+} and Cr^{2+}, corresponding to electronic configurations of d^0, d^1, d^2, d^3 and d^4, respectively. Transition metal ions are usually found in tetrahedral or octahedral coordination, because of their relatively small ionic radii [16]. Symmetries lower than cubic cause a splitting of the energy levels. For example, in tetrahedrally coordinated Cr^{4+} doped yttrium oxyorthosilicate crystals with trigonal symmetry, the $^3T_1(^3F)$ level splits into two closely spaced absorption peaks [17]. This sort of splitting is not evident in our absorption spectrum, therefore we assume ideal

octahedral or tetrahedral coordination. The d^0 electronic configuration results in high energy charge-transfer transitions. In the case of Cr^{6+} doped silicate glasses, a 360 nm absorption band is observed [18]. This could account for our 360 nm absorption band, but not the other two spin allowed transitions. The d^1 configuration can be discounted because there is only one excited state [19], which is incompatible with our five observed absorption bands. The d^4 configuration can be discounted because there would either be one spin allowed transition, or characteristic narrow R-line emission [15], neither of which was observed. This leaves octahedral d^2, tetrahedral d^2, octahedral d^3 and tetrahedral d^3 configurations. Inspection of their Tanabe-Sugano diagrams [20-22] shows we can eliminate tetrahedral d^2 because there is only one spin forbidden transition overlapping the first spin allowed transition, whereas we see two (see Fig. 2). Tanabe-Sugano diagrams use the B and C Racah parameters, which describe the electrostatic interaction strength between multiple 3d electrons [22], and Dq, which is 1/10 the energy of the lowest spin allowed absorption transition. Plotting Tanabe-Sugano diagrams and calculating the crystal field strength (Dq/B) can further elucidate the configuration. To plot the Tanabe-Sugano diagrams we obtained the energy terms, as a function of Dq/B, of each state of each configuration by diagonalizing the energy matrices [20] of these states. To calculate Dq/B, we used the position of the two lowest energy spin allowed absorption bands in Fig. 1 and solved simultaneously the energy terms of the two lowest spin allowed states for each configuration. For octahedral d^2 we found $Dq/B = 2.9$ and is in a strong field site, i.e. the lowest energy transition is a spin forbidden transition. In this case we would see narrow R-line emission, which wasn't observed. The methodology we used for calculating the crystal field strength for the octahedral d^2 configuration is given in Appendix A. For the tetrahedral d^3 configuration, no solution was found when simultaneously solving the energy terms. The octahedral d^2 and tetrahedral d^3 configurations are therefore discounted. For the octahedral d^3 configuration we found $Dq/B=1.99$, and the two spin forbidden states are close to the first spin

allowed state, which is what we would expect from the Fano antiresonance observation. The octahedral d^3 (Cr^{3+}) configuration is therefore the most likely configuration for the Cr ion and is illustrated in the Tanabe-Sugano diagram in Fig. 3. The Racah B parameter was B = 792.2 cm^{-1} , this is relatively high compared to other Cr^{3+} doped glasses [23], indicating a relatively low degree of covalency of the Cr-O bond. The Racah C parameter was calculated from the spin forbidden transitions, which gave C = 3005 cm^{-1}. The ratio, C/B = 3.79, is slightly lower than the expected range of ~ 4 to 5 [20], but is explained by the finding that, contrary to previous assumptions, the Racah C parameter is affected less by the degree of covalency than the Racah B parameter [24], so the relatively low covalency of our glass would tend to push the C/B ratio below the expected range. In addition, the spectral data of various Cr^{3+} doped crystals [25] and glasses [14, 26, 27] is consistent with our absorption and emission spectra. From Fig. 3, the predicted energy of the $^4A_2(^4F) \rightarrow {}^4T_1(^4P)$ transition is 36440 cm^{-1} (275 nm), which is far higher energy than the 360 nm absorption band in Fig. 1, confirming that this band is not associated with octahedral Cr^{3+}, and is most likely associated with a Cr^{6+} charge transfer transition.

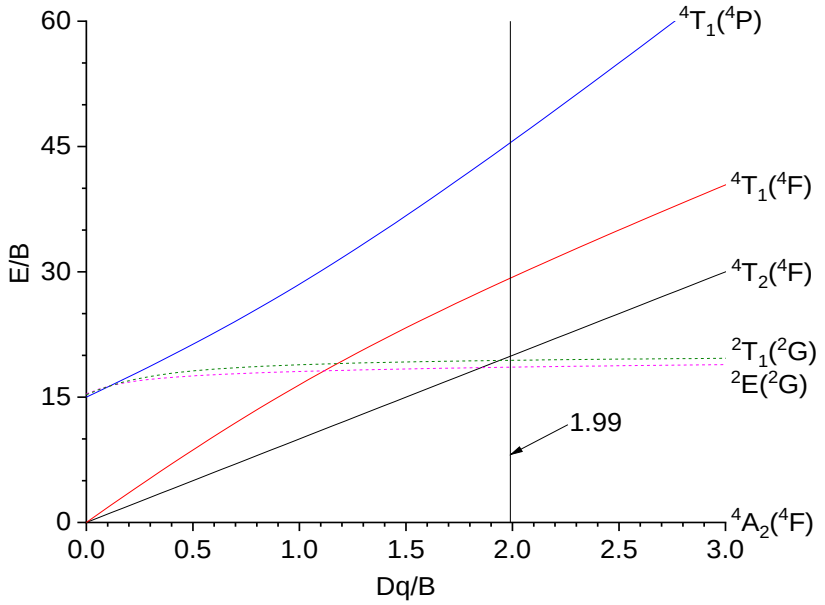

Figure 3. Tanabe-Sugano diagram of Cr-doped SBNACZ glass. The vertical line indicates the crystal field strength.

Fig. 3 shows the octahedral d^3 Tanabe-Sugano diagram calculated with C/B = 3.79, which represents Cr doped SBNACZ glass at the indicated crystal field strength. Using Fig. 3, we can assign the two spin-forbidden absorption bands at 649 and 681 nm to the $^4A_2(^4F)\rightarrow {}^2T_1(^2G)$ and $^4A_2(^4F)\rightarrow {}^2E(^2G)$ transitions, respectively, also, the 432 and 635 nm spin allowed absorption bands are assigned to transitions from the $^4A_2(^4F)$ ground state to the $^4T_1(^4F)$ and $^4T_2(^4F)$ states, respectively.

The energies of all the states predicted by Fig. 3 are consistent with those observed in the absorption spectra in Figs. 1 and 2. The Dq/B is found to be close to the crossing point of the $^4T_2(^4F)$ and $^2T_1(^2G)$ energy curves. Dq/B values of 1.98-2.15 were reported for other Cr^{3+} doped silicate glasses, and the lower value was attributed to the larger modifier ions which lowered the oxygen packing density and increased the predominance of the low-field sites. In our glass the low Dq/B value can be caused by Na^+ and Ca^{2+} which have much larger ionic radii than the other modifier ions.

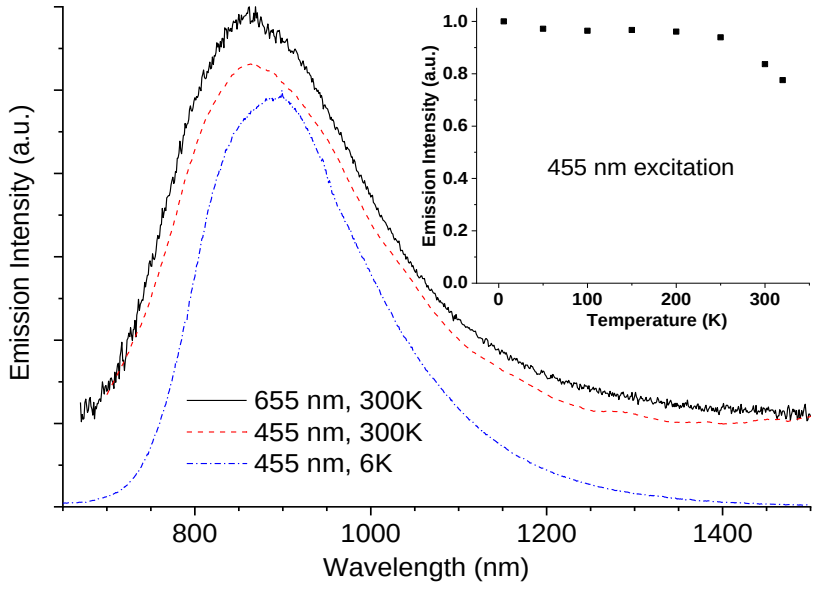

Figure 4. Emission spectra of 0.1 mol.% Cr_2O_3 doped SBNACZ glass at various excitation wavelengths and temperatures. The 300 K spectra are offset for clarity. The inset shows the integrated emission intensity as a function of temperature when exited at 455 nm.

The emission spectra of 0.1 mol.% Cr_2O_3 doped SBNACZ glass are shown in Fig. 4. When excited at 655 nm, the room temperature spectrum exhibits a broad band in the region of 690-1400 nm, peaking at 855 nm and with a full width of half maximum (FWHM) ~250 nm, which is assigned to the $^4T_2(^4F) \rightarrow ^4A_2(^4F)$ transition of the Cr^{3+} ions in weak crystal field sites [14, 28]. The QE of this emission was measured to be 0.6% ± 0.1%. The lack of the R-line emission is consistent with the low Dq/B value [29]. Using the stokes shift (SS) between absorption, and emission bands and the main phonon energy for SBNACZ glass ($\hbar\omega$) of 975 cm^{-1} [8], we can estimate the Huang-Rhys parameter, S_0, from $SS=(2S_0-1)\,\hbar\omega$ [30] to be 2.7, which is in the weak electron-phonon coupling regime and compares to S_0 of 4.5, 3.9 and 4.4 for Cr^{3+} doped phosphate [31], fluoride [32] and silicate glass [33], respectively. The relatively low S_0 of Cr^{3+} doped SBNACZ indicates a relatively low multi-phonon non-radiative relaxation rate, and that the relatively low QE is caused by another process, such as cross-relaxation.

Very similar emission is obtained with 455 nm excitation, indicating that 455 and 655 nm excitation both excite the same Cr centre. Fig. 4 also shows the emission obtained under 455 nm excitation at a temperature of 6 K. Here the peak has red-shifted slightly to 890 nm and the FWHM has reduced to 220 nm. One would usually expect a shift to longer wavelengths as temperature increases, as a result of lattice expansion which would reduce the crystal field strength around the Cr^{3+} ions [28]. However, the same anomalous shift to shorter wavelengths with increasing temperature has been observed in many other Cr^{3+} doped glasses and is attributed to non-radiative decay preferentially affecting the low-energy side of the emission band over the high energy side [14].

The inset of Fig 4 shows the intensity of the emission, detected at 960 nm and excited at 455 nm, as a function of temperature normalized to that observed at 6 K. The figure shows a relatively moderate 20% decrease in emission intensity as the temperature is increased from

6 to 300 K. This compares to an intensity decrease of 70% to 80% [28] observed in Cr^{3+} doped silicate glass. It can also be seen that the emission intensity does not decrease significantly until the temperature reaches ~ 200 K. This indicates that non-radiative decay caused by phonon-coupling does not occur until ~ 200 K. Little difference was observed between the room and cryogenic temperature absorption spectra of a Cr^{3+} doped silicate glass [23], so assuming there is also no change in absorption in our glass, the small increase in emission intensity indicates that there is a smaller increase in QE, and smaller decrease in non-radiative decay by phonon emission as temperature decreases compared to other silicate glasses.

3.2. Cr and Nd co-doped SBNACZ glasses

Fig. 5(a) shows the absorption spectrum of 0.1 mol.% Nd_2O_3 doped glass with four characteristic Nd^{3+} absorption bands at 578, 745, 800 and 870 nm. These bands are ascribed to the transitions from the $^4I_{9/2}$ ground state to the $^2G_{7/2}$, $^4F_{7/2}$, $^4F_{5/2}$ and $^4F_{3/2}$ excited states, respectively [34]. The absorption spectrum of 0.1 mol.% Nd_2O_3 and 0.1 mol.% Cr_2O_3 doped glass is shown in Fig. 5(b), with the narrow Nd^{3+} absorption bands superimposed on the broader Cr^{3+} absorption band. The baseline absorption of the Cr-containing glass is higher than that for the Nd-containing glass. We speculate this is due to residual Cr absorption or Cr lowering the transparency of the glass.

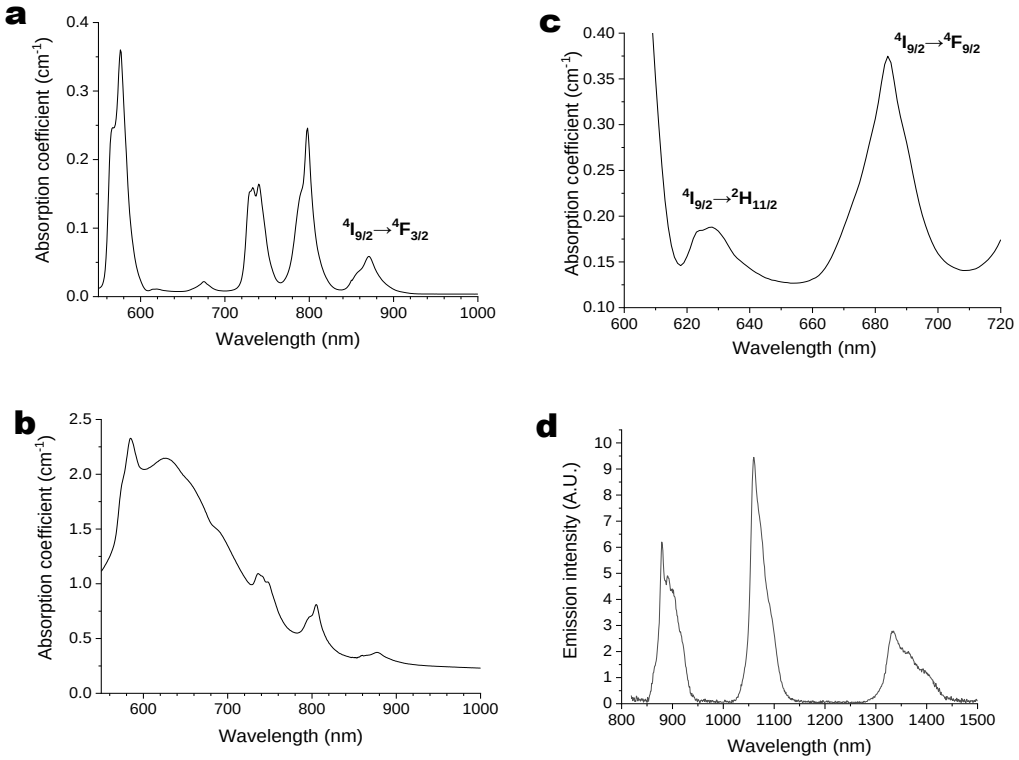

Figure 5. a) Absorption spectrum of 0.1 mol.% Nd_2O_3 doped SBNACZ glass. b) Absorption spectrum of 0.1 mol.% Nd_2O_3 and 0.1 mol.% Cr_2O_3 co-doped SBNACZ glass. c) Close-up of the minimum absorption of 1.0 mol.% Nd_2O_3 doped SBNACZ glass. d) The emission spectrum of 0.1 mol.% Nd_2O_3 doped SBNACZ glass, excited at 808 nm.

For Nd^{3+} singly doped glass, Nd^{3+} absorption is at a minimum at 655 nm, see Fig. 5(c) for the spectrum of 1.0 mol.% Nd_2O_3 doped glass. In contrast, significant absorption occurs at 655 nm for Cr singly doped glass (see Fig.1). Therefore, the 655 nm excitation should only excite the Cr^{3+} ions in the co-doped glass. The emission spectrum of the co-doped glass under 655 nm excitation was found to be indistinguishable from the emission spectrum obtained for Nd singly doped glass when excited at 808 nm, shown in Fig. 5(d). Comparisons between Cr and Nd co-doped and Nd singly doped glasses showed that ~ 2% of the emission from the co-doped glass came from Nd^{3+} directly excited at 655 nm. This confirms that the energy is transferred from the excited Cr^{3+} ions to the Nd^{3+} ions in the co-doped glass.

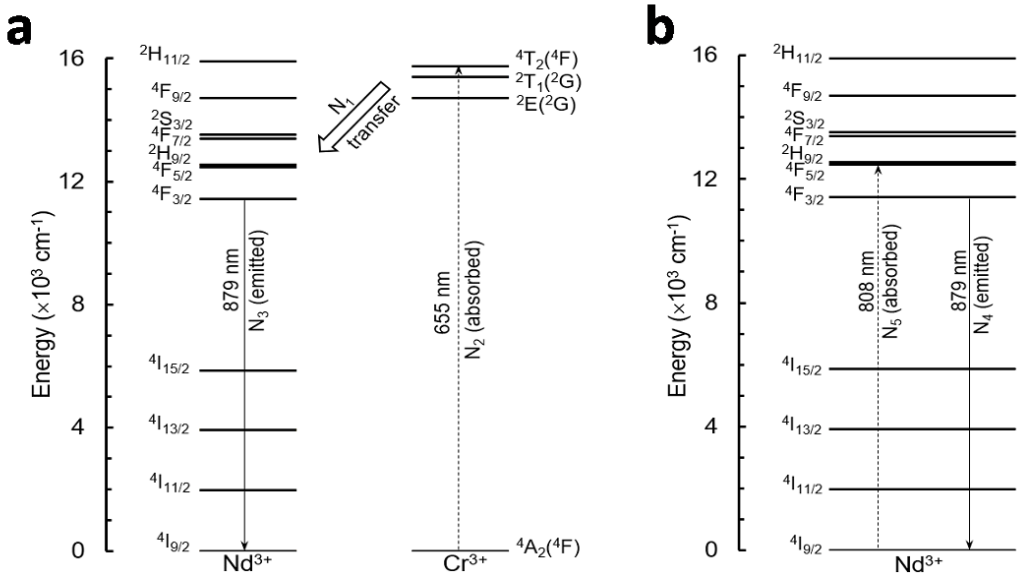

Figure 6. Energy level diagrams for a) Cr^{3+} and Nd^{3+} in co-doped glass under 655 nm excitation and b) Nd^{3+} in singly doped glass under 808 nm excitation.

The $Cr^{3+} \rightarrow Nd^{3+}$ energy transfer efficiency can be measured using the relative fluorescence intensity, lifetime or quantum efficiency of Cr^{3+} donor ions, in the absence and presence of Nd^{3+} acceptor ions. This method assumes the reduction in the Cr^{3+} fluorescence intensity, lifetime, or quantum efficiency is solely due to energy transfer, which can be misleading. It was reported that using the reduction in donor lifetime for the transfer efficiency calculation resulted in much higher values than those measured by the sensitised emission method [35], i.e. using the relative increase in the acceptor emission, in the absence and presence of the donor. Here we use a method to calculate the $Cr^{3+} \rightarrow Nd^{3+}$ energy transfer efficiency by comparing the QE of Cr and Nd co-doped glass excited at 655 nm, with that of Nd singly doped glass excited at 808 nm with the same Nd concentration. The 655 nm laser was used to illuminate a co-doped glass at room temperature, as illustrated in the energy level structure diagram in Fig. 6a. The energy is transferred from Cr^{3+} to Nd^{3+} through the $^4A_2(^4F) \rightarrow {}^4T_2(^4F)$ transition of Cr^{3+}. The transfer QE is:

$$\eta_{tr}=N_1/N_2 \quad (3)$$

where N_1 is the relative number of photons and/or electrons transferred from Cr^{3+} to Nd^{3+}, and N_2 is the relative number of photons absorbed by Cr^{3+}. N_3 is the relative number of photons emitted by Nd^{3+}, and the QE of the co-doped glass, η_{co}, is defined as:

$$\eta_{co}=N_3/N_2 \quad (4)$$

The QE of the Nd^{3+} luminescence in the co-doped glass is:

$$\eta_{Nd1}=N_3/N_1 \quad (5)$$

At room temperature the 808 nm laser was used to excite Nd^{3+} in the Nd singly doped glass with the same Nd content as the co-doped glass (Fig. 6b). The QE of the Nd^{3+} luminescence in the singly doped glass is:

$$\eta_{Nd2}=N_4/N_5 \quad (6)$$

where N_4 is the relative number of photons emitted by Nd, and N_5 is the relative number of photons absorbed by Nd. Our method relies on the assumption that the QE of Nd^{3+} is the same in the singly and co-doped glasses, which is reasonable given the very low Cr_2O_3 concentration in the co-doped glass. Thus, $\eta_{Nd1}=\eta_{Nd2}$, and:

$$\eta_{tr}=\eta_{co}/\eta_{Nd2} \quad (7)$$

To perform such analysis each η_{tr} measurement requires a pair of samples: a co-doped glass and a Nd_2O_3 singly doped glass with the same Nd_2O_3 concentration as in the co-doped glass. We prepared three such pairs of samples with a fixed Cr_2O_3 concentration of 0.1 mol.%, and varying Nd_2O_3 concentrations of 0.1, 0.5 and 1 mol.%.

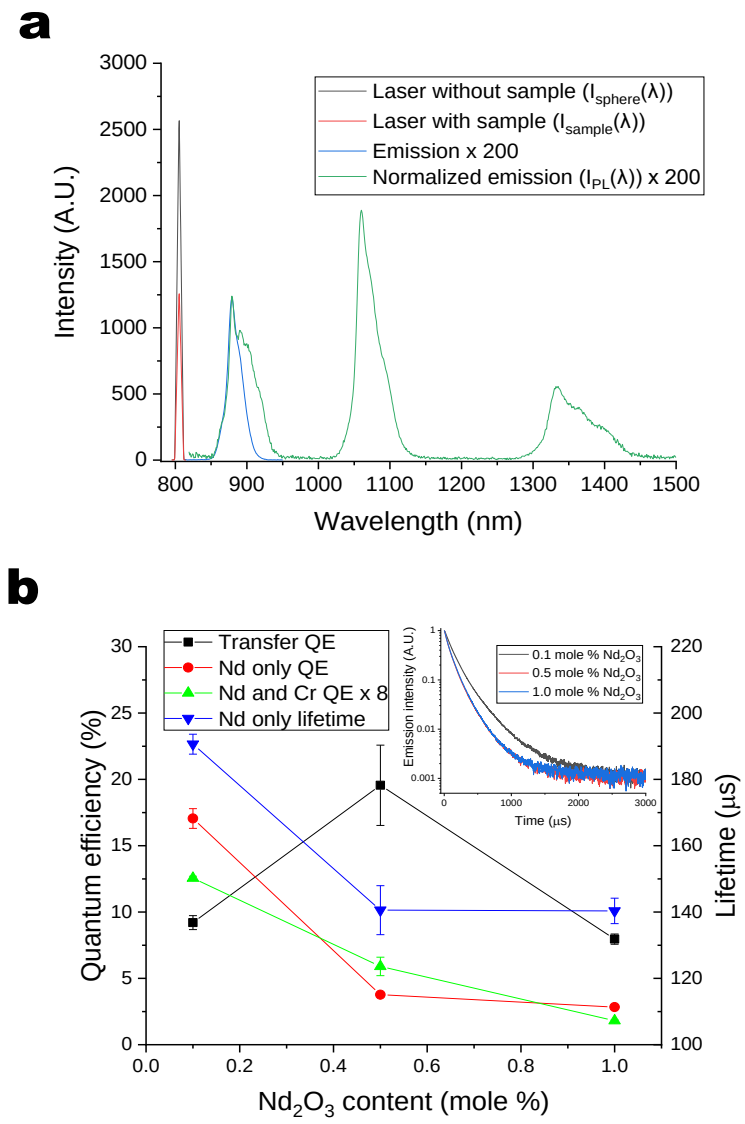

Figure 7. a) An example of the spectra used to calculate the QE for 0.1 mol.% Nd_2O_3 doped SBNACZ glass, excited at 808 nm, showing the laser line with and without the sample present, the emission collected on the QE system, and the normalized Nd^{3+} emission spectrum used for the QE calculation, scaled by a factor of 200 are also shown. b) Lifetime, QE and transfer QE of Nd and Cr co-doped SBNACZ glass as a function of Nd content. The QE and lifetime of Nd singly doped SBNACZ glass as a function of Nd content is also shown. The inset shows the emission decay profiles of Nd singly doped SBNACZ glass.

Fig. 7 (a) Shows an example of the spectra used to calculate the QE, in this case for 0.1 mol.% Nd_2O_3 doped SBNACZ glass, excited at 808 nm. The QE measurement requires the same detector for laser and emission spectra, however, neither the PMT or InGaAs detector could cover the 655 and 808 nm laser lines and the first three Nd^{3+} emission bands, so we used the PMT detector, which had a cut-off at ~ 900 nm, for the QE measurements and normalized the emission spectrum collected using the InGaAs detector to that collected with the PMT detector, as shown in Fig. 7 (a), and used the normalized spectrum for the QE calculation.

Fig. 7 (b) shows the changes of and η_{tr}, η_{co} and η_{Nd2} with the content of Nd_2O_3. It is noteworthy that η_{tr} first increases when the Nd_2O_3 content is increased from 0.1 to 0.5 mol.% and then decreases when the Nd_2O_3 content is increased from 0.5 to 1.0 mol.%. η_{tr} reaches a maximum value of 20% at 0.5 mol.% Nd_2O_3.

The inset of Fig. 7(b) shows the decay profiles of the 1064 nm emission band of the Nd singly doped glass when excited at 808 nm for various Nd_2O_3 concentrations. The decays are highly non-exponential, as is commonly observed in disordered materials such as glasses[36-39]. The lifetime, calculated using Eq. 1, drops from 190 μs to 140 μs as the Nd_2O_3 content is increased from 0.1 to 0.5 mol.%, but changes very little as the Nd_2O_3 content is increased further to 1 mol.%. This indicates that the reduction in lifetime at 0.5% Nd is caused by clustering, and as the Nd content is increased to 1% no further clustering occurs. We have previously found evidence of Nd clustering in a similar Nd doped glass[40]. Fig. 7(b) also shows the QE of the Nd singly doped SBNACZ glass when excited at 808 nm and the QE of the Nd and Cr co-doped SBNACZ glass as a function of Nd content. The QE of the Nd singly doped glass follows a similar pattern to its lifetime, with a significant fall as the Nd_2O_3 content is increased from 0.1 to 0.5 mol.%, but with little change again as the Nd_2O_3 content is increased to 1 mol.%. The increase in transfer QE as Nd_2O_3 content is increased from 0.1 to 0.5% is expected since a decrease in Cr^{3+}-Nd^{3+} separation would increase the transfer rate.

However, it is somewhat unexpected that the transfer QE then reduces as the Nd_2O_3 content is increased to 1%. In Cr and Nd co-doped fluorophosphate glass [41] and $YAl_3(BO_3)_4$ [42] the transfer QE increased continuously with increasing Nd content. A possible explanation for this is the Nd^{3+} clustering that seems to occur at 0.5 mol.% Nd_2O_3; these clusters could form defect sites that quench excitation from Cr^{3+} non-radiatively, before it can be transferred to Nd^{3+} ions that are not in defect sites. If the proximity of these Nd^{3+} cluster defects to Cr only becomes significant at 1 mol.% Nd_2O_3, this would explain the drop in transfer QE at 1 mol.% Nd_2O_3. The maximum transfer QE of 20% reported in this work compares to a maximum of 4.7% for SiO_2-Na_2O-K_2O glass with 0.1 mol.% Cr_2O_3 and 0.2 mol.% Nd_2O_3 [43].

Energy transfer from a donor to an acceptor can occur via radiative or non-radiative mechanisms. As the absorption strength of the donor is usually small for inorganic systems, radiative transfer is not often encountered [44], and the low absorption cross section of Nd^{3+} makes this even more unlikely. Strong non-radiative energy transfer can occur via two different resonance mechanisms: the Förster mechanism (coulombic interaction) and the Dexter mechanism (electron exchange) [45-47]. The coulombic interaction mechanism is effective over a donor-acceptor distance of 1-10 nm, whereas the electron exchange mechanism is operative for a donor-acceptor distance of less than 1 nm [48]. For both mechanisms, the energy transfer rate increases with decreasing donor-acceptor distance.

The lower limit of the average Cr^{3+}-Nd^{3+} separation can be estimated from the molar composition of the glass and its density. For the co-doped glasses with Nd_2O_3 concentrations of 0.1, 0.5 and 1 mol.%, we obtain Cr^{3+}-Nd^{3+} average separations of 2.3 nm, 1.6 nm and 1.3 nm, respectively, indicating that the coulombic interaction mechanism is the dominant $Cr^{3+}\rightarrow Nd^{3+}$ transfer mechanism in all our glasses. The efficiency of this interaction mechanism is influenced by the overlap integral of acceptor absorption and donor emission cross-sections [49]. From Fig. 4 and Fig. 5 (a), we see the Cr^{3+} the $^4T_2(^4F) \rightarrow ^4A_2(^4F)$ emission transition,

peaking at 855 nm matches the $^4I_{9/2} \rightarrow {}^4F_{3/2}$ absorption transition of Nd^{3+} at 870 nm; however, the greater bandwidth of the Cr^{3+} emission may be a limiting factor for transfer efficiency.

If Nd^{3+} clustering occurs, or we take into account the proportion of Cr that becomes Cr^{6+}, Cr^{3+}-Nd^{3+} separations would be higher than our estimates. However, this would still imply the coulombic interaction mechanism is dominant. By further optimizing the Cr and Nd^{3+} doped SBANCZ glass system by adjusting the glass composition, doping concentrations and melting conditions so the Cr^{3+}/Cr^{6+} ratio is maximized and Nd^{3+} clustering at high concentrations is minimized, this glass system could be a suitable platform for developing SPLs.

4. Conclusions

We used Tanabe-Sugano analysis and comparisons to previous work to determine that when Cr doped SBNACZ glass contains Cr^{3+} in octahedral coordination and Cr^{6+} with unknown coordination. Cr doped SBNACZ glass displays three broad absorption bands centered at 360, 432 and 642 nm which are attributed to a Cr^{6+} charge transfer transition, and spin allowed transitions to the $^4T_1(^4F)$ and $^4T_2(^4F)$ states of Cr^{3+}, respectively. There are also two narrow spin forbidden absorption bands at 649 and 681 nm, which are attributed to transitions to the $^2T_1(^2G)$ and $^2E(^2G)$ states of Cr^{3+}, respectively. Emission, when excited at both 455 and 655 nm, peaks at 855 nm with a FWHM of 250 nm. The QE of this emission was 0.6%, and its intensity increased by 20% when cooled to cryogenic temperatures. The Racah B parameter for Cr^{3+} was B=792.2 cm^{-1}, which is relatively low, indicating a relatively low degree of covalency of the Cr-O bond. The crystal field strength (Dq/B=1.99) was also relatively low, which could be caused by Na^+ and Ca^{2+} which have much larger ionic radii than other commonly used modifier ions. We also calculated a relatively low C/B ratio (3.79); however,

this is consistent with the expected range. The broad Cr^{3+} emission band is due to the $^4T_2(^4F) \rightarrow ^4A_2(^4F)$ transition of Cr^{3+} in weak crystal field sites, where the lowest energy transition is spin allowed.

For the co-doped SBNACZ glass, the Nd^{3+} absorption bands were found to be superimposed on the broader Cr^{3+} absorption band. The $Cr^{3+} \rightarrow Nd^{3+}$ energy transfer efficiency was calculated using a method comparing the QE of co-doped and singly doped glasses with the same Nd^{3+} concentration. With the Cr_2O_3 content fixed at 0.1 mol.%, the transfer efficiency first increases when the Nd_2O_3 content is increased from 0.1 to 0.5 mol.%, due to the reduced Cr^{3+}-Nd^{3+} separation, and then decreases when the Nd_2O_3 content is increased from 0.5 to 1.0 mol.%, due to Nd^{3+} cluster defect sites that quench excitation from Cr^{3+} non-radiatively. A maximum transfer QE of 20% has been obtained at 0.5 mol.% Nd_2O_3. The $Cr^{3+} \rightarrow Nd^{3+}$ energy transfer is dominated by the coulombic interaction mechanism at all the Nd_2O_3 concentrations investigated. Because of the very high rare earth solubility of SBNACZ glass, Cr and Nd^{3+} co-doped SBNACZ glass is a promising candidate for SPLs, particularly if the issue of Nd^{3+} clustering at higher concentrations can be overcome. Future work could involve optimizing the glass composition and melting conditions to minimize Nd^{3+} clustering at higher concentrations.

Disclosure statement

No potential conflict of interest was reported by the authors.

Data Availability

The data used in this article is available from the corresponding author upon request.

References

[1] T. Yabe, S. Uchida, K. Ikuta, K. Yoshida, C. Baasandash, M.S. Mohamed, Y. Sakurai, Y. Ogata, M. Tuji, Y. Mori, Y. Satoh, T. Ohkubo, M. Murahara, A. Ikesue, M. Nakatsuka, T.

Saiki, S. Motokoshi, C. Yamanaka, Demonstrated fossil-fuel-free energy cycle using magnesium and laser, Appl. Phys. Lett., 89 (2006) 261107.
[2] H. Yagi, T. Yanagitani, H. Yoshida, M. Nakatsuka, K. Ueda, Highly efficient flashlamp-pumped Cr^{3+} and Nd^{3+} codoped $Y_3Al_5O_{12}$ ceramic laser, Jpn. J. Appl. Phys., 45 (2006) 133-135.
[3] T. Kato, H. Ito, K. Hasegawa, T. Ichikawa, A. Ikesue, S. Mizuno, Y. Takeda, A. Ichiki, T. Motohiro, Effect of Cr content on the output of a solar-pumped laser employing a Cr-doped Nd: YAG ceramic laser medium operating in sunlight, Jpn. J. Appl. Phys., 58 (2019) 062007.
[4] T. Yabe, T. Ohkubo, S. Uchida, K. Yoshida, M. Nakatsuka, T. Funatsu, A. Mabuti, A. Oyama, K. Nakagawa, T. Oishi, K. Daito, B. Behgol, Y. Nakayama, M. Yoshida, S. Motokoshi, Y. Sato, C. Baasandash, High-efficiency and economical solar-energy-pumped laser with Fresnel lens and chromium codoped laser medium, Appl. Phys. Lett., 90 (2007) 261120.
[5] I. Bardez, D. Caurant, J.L. Dussossoy, P. Loiseau, C. Gervais, F. Ribot, D.R. Neuville, N. Baffier, C. Fillett, Development and characterization of rare earth-rich glassy matrices envisaged for the immobilization of concentrated nuclear waste solutions, Nuclear Science and Engineering, 153 (2006) 272-284.
[6] T. Yamashita, Y. Ohishi, Concentration and temperature effects on the spectroscopic properties of Tb^{3+} doped borosilicate glasses, J. Appl. Phys., 102 (2007) 123107.
[7] T. Yamashita, Y. Ohishi, Cooperative energy transfer between Tb^{3+} and Yb^{3+} ions co-doped in borosilicate glass, J. Non-Cryst. Solids, 354 (2008) 1883-1890.
[8] T. Yamashita, Y. Ohishi, Analysis of energy transfers between Tb^{3+} and Yb^{3+} codoped in borosilicate glasses, J. Opt. Soc. Am. B, 26 (2009) 819-829.
[9] J. Ren, J. Qiu, D. Chen, X. Hu, X. Jiang, C. Zhu, Ultrabroad infrared luminescence from Bi-doped aluminogermanate glasses, Solid State Commun., 141 (2007) 559-562.
[10] M.A. Hughes, T. Suzuki, Y. Ohishi, Compositional dependence of the optical properties of bismuth doped lead-aluminum-germanate glass, Opt. Mater., 32 (2010) 1028-1034
[11] M. Hughes, T. Suzuki, Y. Ohishi, Towards a high-performance optical gain medium based on bismuth and aluminum co-doped germanate glass, J. Non-Cryst. Solids, 356 (2010) 407-418.
[12] C.E. Finlayson, A. Amezcua, P.J. Sazio, P.S. Walker, M.C. Grossel, R.J. Curry, D.C. Smith, J.J. Baumberg, Infrared emitting PbSe nanocrystals for telecommunications window applications, Journal of Modern Optics, 52 (2005) 955-964.
[13] N.C. Greenham, Measurement of absolute photoluminescence quantum efficiencies in conjugated polymers, Chem. Phys. Lett., 241 (1995) 89-96.
[14] D.L. Russell, K. Holliday, M. Grinberg, D.B. Hollis, Broadening of optical transitions in Cr^{3+}-doped aluminosilicate glasses, Phys. Rev. B, 59 (1999) 13712-13718.
[15] M.A. Hughes, R.J. Curry, D.W. Hewak, Determination of the oxidation state and coordination of a vanadium doped chalcogenide glass, Opt. Mater., 33 (2011) 315–322.
[16] H.P. Christensen, H.P. Jenssen, Broad-band emission from chromium doped germanium garnetes, IEEE J. Quantum Electron., 18 (1982) 1197-1201
[17] C. Deka, M. Bass, B.H.T. Chai, Y. Shimony, Optical spectroscopy of Cr^{4+}:Y_2SiO_5, J. Opt. Soc. Am. B, 10 (1993) 1499.
[18] M. Casalboni, V. Ciafardone, G. Giuli, B. Izzi, E. Paris, P. Prosposito, An optical study of silicate glass containing and ions, J. Phys.-Condes. Matter, 8 (1996) 9059.
[19] J.P. Meyn, T. Danger, K. Petermann, G. Huber, Spectroscopic characterisation of V^{4+} doped Al_2O_3 and $YAlO_3$, J. Lumines., 55 (1993) 55-62.
[20] Y. Tanabe, S. Sugano, On the Absorption Spectra of Complex Ions, Journal of the Physical Society of Japan, 9 (1954) 753-779.
[21] S. Sugano, Y. Tanabe, H. Kamimura, Multiplets of transition-metal ions in crystals Academic Press, New York, 1970.

[22] B. Henderson, G.F. Imbusch, Optical spectroscopy of inorganic solids, Oxford University Press, Oxford, 1989.
[23] F. Rasheed, K.P. O'Donnell, B. Henderson, D.B. Hollis, Disorder and the optical spectroscopy of Cr^{3+} doped glasses: 1. Silicate glasses, J. Phys.-Condes. Matter, 3 (1991) 1915-1930.
[24] M. Atanasov, C. Daul, C. Rauzy, New insights into the effects of covalency on the ligand field parameters: a DFT study, Chem. Phys. Lett., 367 (2003) 737-746.
[25] S. Kuck, Laser-related spectroscopy of ion-doped crystals for tunable solid-state lasers, Applied Physics B: Photophysics and Laser Chemistry, 72 (2001) 515-562.
[26] L.J. Andrews, A. Lempicki, B.C. McCollum, Spectroscopy and photokinetics of chromium (III) in glass, J. Chem. Phys., 74 (1981) 5526-5538.
[27] C.R. Mendonca, B.J. Costa, Y. Messaddeq, S.C. Zilio, Optical properties of chromium-doped fluoroindate glasses, Phys. Rev. B, 56 (1997) 2483-2487.
[28] B. Henderson, M. Yamaga, Y. Gao, K.P. Odonnell, Disorder and Nonradiative Decay of Cr^{3+}-Doped Glasses, Phys. Rev. B, 46 (1992) 652-661.
[29] F. Rasheed, K.P. Odonnell, B. Henderson, D.B. Hollis, Disorder and the Optical Spectroscopy of Cr^{3+} Doped Glasses: .2. Glasses with High and Low Ligand-Fields, J. Phys.-Condes. Matter, 3 (1991) 3825-3840.
[30] M. de Jong, L. Seijo, A. Meijerink, F.T. Rabouw, Resolving the ambiguity in the relation between Stokes shift and Huang–Rhys parameter, PCCP Phys. Chem. Chem. Phys., 17 (2015) 16959-16969.
[31] M. Haouari, M. Ajroud, H. Ben Ouada, H. Maaref, A. Brenier, C. Garapon, Spectroscopic Properties of Cr^{3+} - Doped Phosphate Glasses, Physica status solidi (b), 215 (1999) 1165-1177.
[32] M.A. Illarramendi, J. Fernández, R. Balda, J. Lucas, J.L. Adam, Optical spectroscopy of Cr^{3+} doped fluoride BIGaZYT glass, J. Lumines., 47 (1991) 207-216.
[33] U.R. Rodríguez-Mendoza, V. Lavín, I.R. Martín, V.D. Rodríguez, Optical properties and site distribution of Cr^{3+} ions in alkali-disilicate glasses, J. Lumines., 106 (2004) 77-90.
[34] G.H. Dieke, H.M. Crosswhite, H. Crosswhite, Spectra and energy levels of rare earth ions in crystals, Interscience Publishers, New York,, 1968.
[35] J.G. Edwards, S. Gomulka, Enhanced Performance of Nd Laser Glass by Double Doping with Cr, J. Phys. D-Appl. Phys., 12 (1979) 187-194.
[36] M.A. Hughes, K.P. Homewood, R.J. Curry, Y. Ohishi, T. Suzuki, Waveguides in Ni-doped glass and glass–ceramic written with a 1kHz femtosecond laser, Opt. Mater., 36 (2014) 1604-1608.
[37] M. Hughes, D.W. Hewak, R.J. Curry, Concentration dependence of the fluorescence decay profile in transition metal doped chalcogenide glass, in: Photonics West, SPIE Photonics West, San Jose, USA, 2007.
[38] M. Hughes, H. Rutt, D. Hewak, R. Curry, Spectroscopy of vanadium (III) doped gallium lanthanum sulphide glass, Appl. Phys. Lett., 90 (2007) 031108.
[39] M. Hughes, T. Suzuki, Y. Ohishi, Advanced bismuth doped lead-germanate glass for broadband optical gain devices, J. Opt. Soc. Am. B, 25 (2008) 1380-1386
[40] T. Suzuki, H. Nasu, M. Hughes, S. Mizuno, K. Hasegawa, H. Ito, Y. Ohishi, Quantum efficiency measurements on Nd-doped glasses for solar pumped lasers, J. Non-Cryst. Solids, 356 (2010) 2344-2349.
[41] R. Balda, J. Fernández, A. de Pablos, J.M. Fernández-Navarro, Cr^{3+} Nd^{3+} energy transfer in fluorophosphate glass investigated by time-resolved laser spectroscopy, Phys. Rev. B, 48 (1993) 2941.
[42] E. Bovero, E. Cavalli, D. Jaque, J.G. Sole, A. Speghini, M. Bettinelli, Cr^{3+}-> Nd^{3+} energy transfer in the $YAl_3(BO_3)_4$ nonlinear laser crystal, J. Appl. Phys., 98 (2005) 023103.

[43] S. Mizuno, H. Nasu, M. Hughes, T. Suzuki, H. Ito, K. Hasegawa, Y. Ohishi, The efficiencies of energy transfer from Cr to Nd ions in silicate glasses, in: Photonics West, SPIE Photonics West, San Francisco, 2010.
[44] G. Blasse, Influence of Crystal Structure on Luminescence, Materials Research Bulletin, 3 (1968) 807-815.
[45] D.L. Dexter, A Theory of Sensitized Luminescence in Solids, J. Chem. Phys., 21 (1953) 836-850.
[46] T. Forster, Energiewanderung Und Fluoreszenz, Naturwissenschaften, 33 (1946) 166-175.
[47] T. Forster, Zwischenmolekulare Energiewanderung Und Fluoreszenz, Ann Phys-Berlin, 2 (1948) 55-75.
[48] N. Hildebrandt, I.L. Medintz, FRET-Forster Resonance Energy Transfer: From Theory to Applications, Wiley-VCH Verlag GmbH, 2014.
[49] Y. Zheng, B. Chen, H. Zhong, J. Sun, L. Cheng, X. Li, J. Zhang, Y. Tian, W. Lu, J. Wan, T. Yu, L. Huang, H. Yu, H. Lin, Optical Transition, Excitation State Absorption, and Energy Transfer Study of Er^{3+}, Nd^{3+} Single-Doped, and Er^{3+}/Nd^{3+} Codoped Tellurite Glasses for Mid-Infrared Laser Applications, J. Am. Ceram. Soc., 94 (2011) 1766-1772.

Appendix A

Energy terms of the Octahedral d^2 configuration

The energy terms of the $^3T_2(^3F)$ and $^3A_2(^3F)$ states are 10Dq-8B and 20Dq-8B, respectively [20]. The energy terms of the $^3T_1(^3F,^3P)$ states were calculated by diagonalizing the energy matrix given Table A1, taken from ref [20]. These energy terms were then divided by B, since this is the normalization used in Tanabe-Sugano diagrams. The energy term with the lowest energy ($^3T_1(^3F)$) was then subtracted from all the energy terms to give the energy terms used in the octahedral d^2 Tanabe-Sugano diagram. The first three energy terms with spin allowed transition between them are given in Eqs. A1 to A3; note $E\left(\,^3T_1(\,^3F)\right)/\mathrm{B} = 0$. To calculate Dq/B, Dq is 1/10 of the energy of the lowest spin allowed absorption transition. Therefore, B is calculated from the energies of the $^3T_2(^3F)$ and $^3T_1(^3P)$ energy levels, determined experimentally, and then solving their energy terms simultaneously for B.

$$E\left(\,^3T_2(\,^3F)\right)/\mathrm{B} = -7.5 + 5\mathrm{Dq/B} + \frac{1}{2}\sqrt{225 + 180Dq/B + 100(Dq/B)^2} \qquad \text{(A1)}$$

$$E\left(\,^3A_2(\,^3F)\right)/\mathrm{B} = -7.5 + 15\mathrm{Dq/B} + \frac{1}{2}\sqrt{225 + 180Dq/B + 100(Dq/B)^2} \qquad \text{(A2)}$$

$$E\left(\,^3T_1(\,^3P)\right)/\mathrm{B} = \sqrt{225 + 180Dq/B + 100(Dq/B)^2} \qquad \text{(A3)}$$

Table A1 energy matrix for the $^3T_1(^3F,^3P)$ state.

t_2^2	t_2e
-5B	6B
6B	10Dq+4B